Supporting Information

Engineering Metal Organic Frameworks for Photoacoustic Imaging Guided Chemo/Photothermal Combinational Tumor Therapy

Ying Zhang [a,c], Lei Wang [b], Liang Liu [a,c], Lin Lin [a], Feng Liu [a,c], Zhigang Xie [b]*, Huayu Tian [a]*, Xuesi Chen [a]

[a] Key Laboratory of Polymer Ecomaterials, Changchun Institute of Applied Chemistry, Chinese Academy of Sciences, Changchun 130022, China

[b] State Key Laboratory of Polymer Physics and Chemistry, Changchun Institute of Applied Chemistry, Chinese Academy of Sciences, Changchun 130022, China

[c] University of Chinese Academy of Sciences, Beijing 100049, China

1. Calculation of the photothermal conversion efficiency

By the following calculation, the photothermal conversion efficiency (η) of MCH NPs was 20.98%.

η could be calculated according to the following equation (eq (1)) (*J. Phys. Chem. C* 2007, *111*, 3636):

$$\eta = \frac{hS\,(T_{max} - T_0) - Q_0}{I(1 - 10^{-A_\lambda})} \times 100\%$$

in which, T_{max}-T_0 was 38.9 °C. Q_0 is the baseline energy input of the sample cell. I was the laser power 1.0 W cm^{-2}. A_{808} was the absorption intensity of MCH NPs at 808 nm, and that was 1.1. h was the heat transfer coefficient. S was the surface area of the sample well. hS can be determined according to the following equation (eq (2)):

$$hS = \frac{\sum_i C_{p,i} m_i}{\tau_s}$$

in which, the weight of MCH NPs solution (m) was 0.2 g, the specific heat capacity value (C) of the solvent (H_2O) was about 4.2 J g^{-1} K^{-1}. τ_s was the slope of the line in **Figure 3F**, which was calculated as 163.18. Substituting hS into eq (1), the η of MCH NPs could be calculated to be 20.98%.

2. XRD spectra

The XRD spectra (**Figure S1**) indicated the successful fabrication of MIL-100. The peak at about 2.5° suggested the amorphous nature of MIL-100. After encapsulated curcumin in the pores of MIL-100, the obtained MC NPs exhibited similar XRD spectra to MIL-100, indicating that the therapeutics loading showed negligible influence on the structure of MIL-100. Finally, after HA-PDA coated on the surface of MC NPs, the weakened peaks in the XRD spectra of MCH NPs suggested the successful surface functionalization of MC NPs.

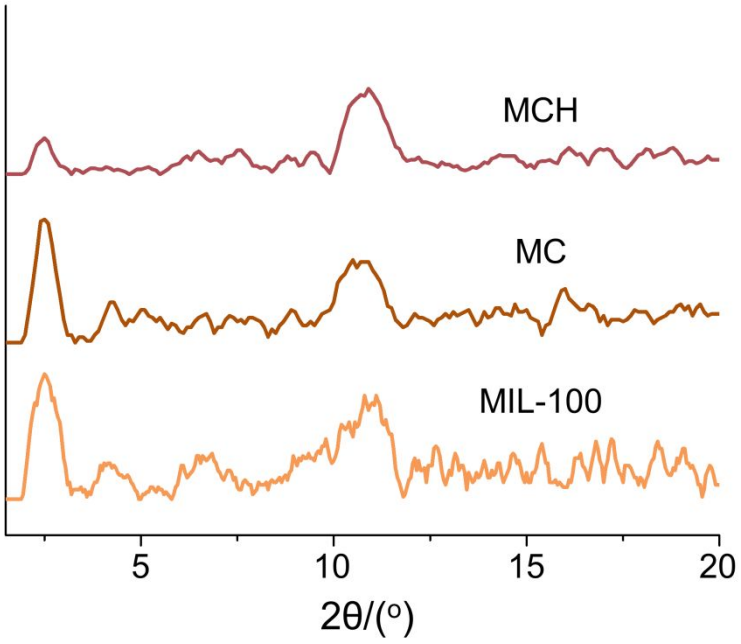

Figure S1. XRD spectra of MIL-100, MC NPs and MCH NPs.

3. Porosity of MIL-100

In the TEM images of MIL-100 in **Figure S2**, the pores of MIL-100 could be clearly observed. This result significantly confirmed the porosity of MIL-100.

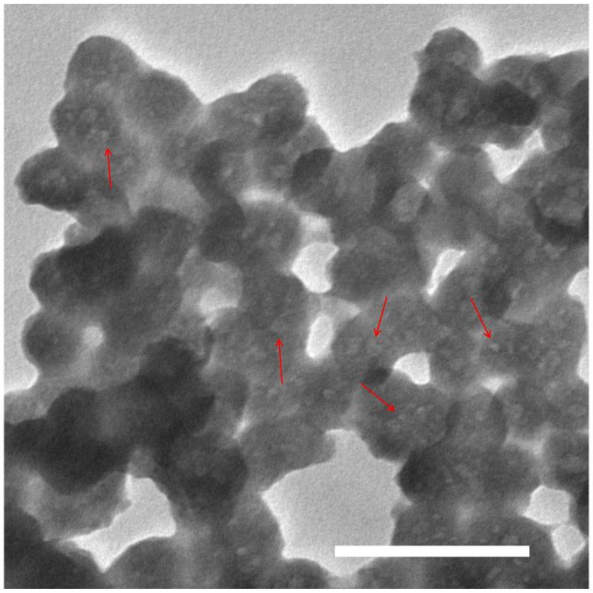

Figure S2. The TEM images of MIL-100. (scale bar: 200 nm)

4. Synthesis of HA-PDA

HA-PDA was synthesized through the reaction of HA-CHO with dopamine hydrochloride under alkaline conditions (**Figure S3**). Briefly, HA-CHO was synthesized according to the previously reported procedure. Then, through the Schiff-base reaction between HA-CHO with dopamine hydrochloride and polymerization of dopamine hydrochloride under alkaline conditions, HA-PDA was obtained and characterized by ^{1}H NMR (**Figure S4**).

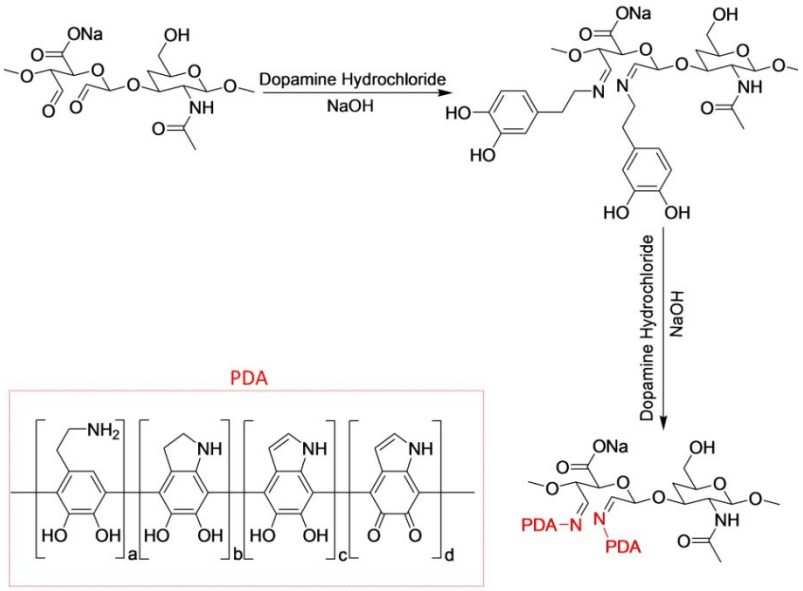

Figure S3. The reaction routes of HA-PDA.

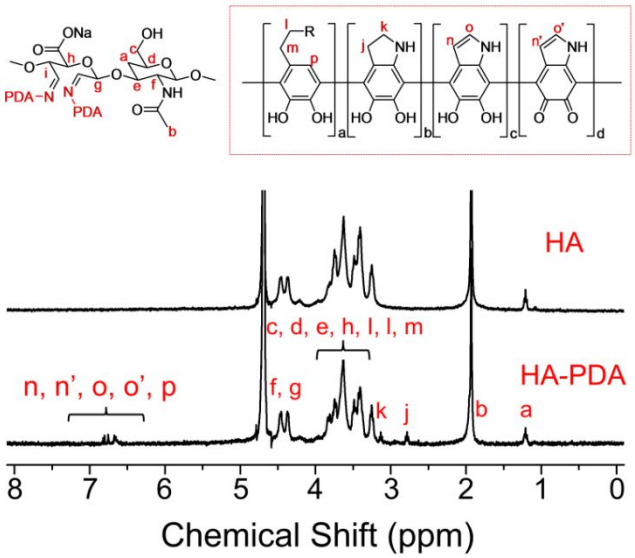

Figure S4. ^{1}H NMR spectra of HA and HA-PDA.

5. FT-IR spectra of MIL-100, MC NPs and MCH NPs

According to the FT-IR spectra shown in **Figure S5**, the curcumin encapsulation and HA-PDA coating could be confirmed. Firstly, compared to MIL-100 and MC NPs, the peaks at about 1720 cm^{-1} that affiliate to the carboxyl groups on BTC were weakened in the spectrum of MCH NPs. And during the drug loading and HA-PDA coating process, the peaks at 1600 cm^{-1} and 1520 cm^{-1} appeared, which affiliated to the C=N bond in HA-PDA and C=C bond in curcumin, respectively. In addition, the peaks corresponding to the methylene in HA-PDA appeared at about 1430 cm^{-1} in the spectrum of MCH NPs. From these results, it could be inferred that curcumin loading and HA-PDA coating were successfully achieved.

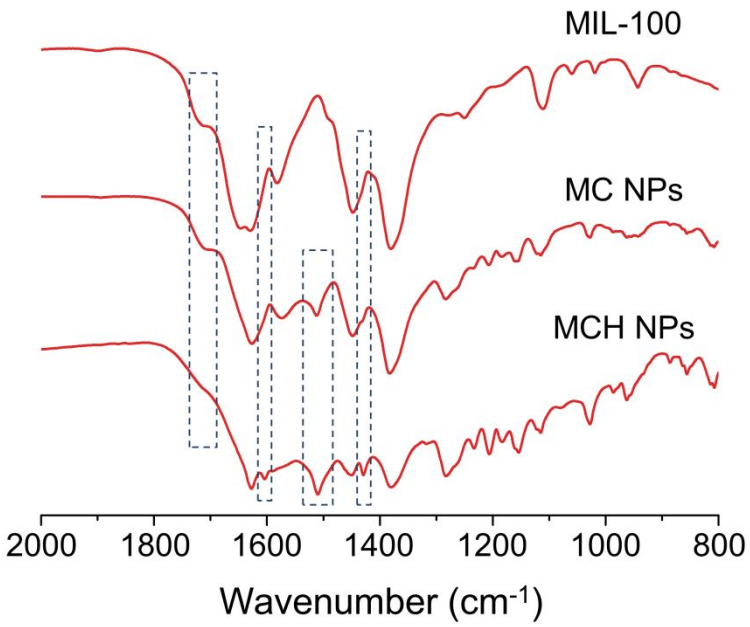

Figure S5. The FTIR spectra of MIL-100, MC NPs and MCH NPs.

6. Photothermal Effect of Fe-curcumin Complexes

To explore the reasons that contributed to the photothermal effect of MC NPs, Fe-curcumin complexes were prepared and used to investigate the photothermal effect under 808 nm laser irradiation (1.0 W/cm^2) (**Figure S6**). The results suggested the excellent photothermal conversion ability of Fe-curcumin complexes, which would be the main reason of the photothermal effect for MC NPs.

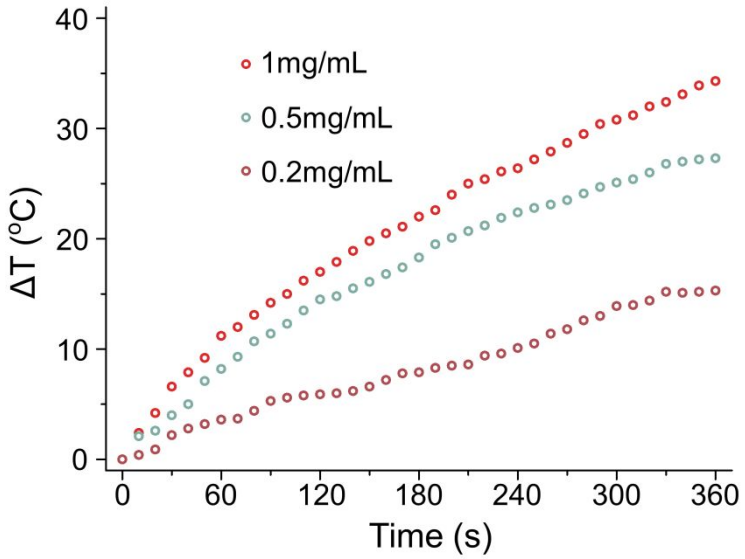

Figure S6. The temperature change of Fe^{3+}-curcumin complexes solutions with different concentrations under 808 nm laser irradiation (1.0 W/cm^2).

7. Infrared Thermographic Images of MCH NPs

The infrared thermographic images were presented to visually confirm the photothermal effect of MCH NPs (**Figure S7**). Under 808 nm laser irradiation (1 W/cm^2), the temperature of MCH NPs solution significantly increased. After 6 min of irradiation, the temperature increased from 28.5 ^{o}C to 68.9 ^{o}C.

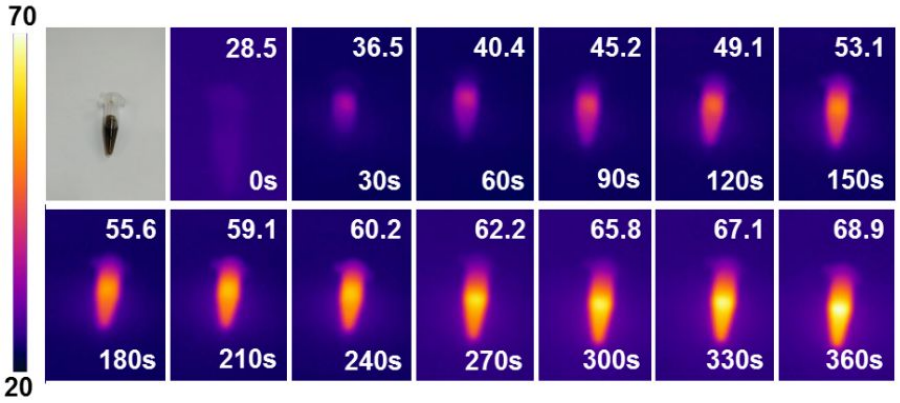

Figure S7. The infrared thermographic images of MCH NPs solution under 808 nm laser irradiation (1.0 W/cm^2). (Unit: ^{o}C)

8. pH Sensitive Cleavage of HA-PDA

When incubated under acidic conditions, MCH NPs exhibited increased zeta potential, indicating the detachment of negatively charged coatings. So it was necessary to investigate the pH sensitive cleavage of HA-PDA. After pH was decreased, the characteristic peaks corresponding to HA-CHO appeared at 4.9-5.3 ppm (**Figure S8**). This result strongly supported the pH sensitive cleavage of HA-PDA.

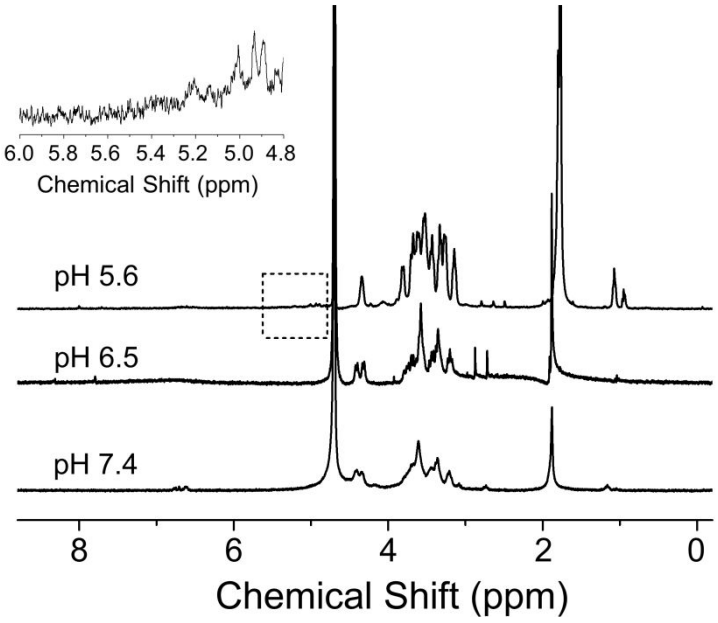

Figure S8. ^{1}H NMR spectra of HA-PDA at different pH.

9. MIL-100 Degradation Study

The degradation of MIL-100 was investigated at different pH (**Figure S9**). At pH 7.4, unobvious degradation was detected for MIL-100. However, when incubated at acidic conditions, the degradation of MIL-100 accelerated, displaying an acid-triggered degradation behavior. This could be beneficial for MCH NPs to realize pH-sensitive drug release at tumor site.

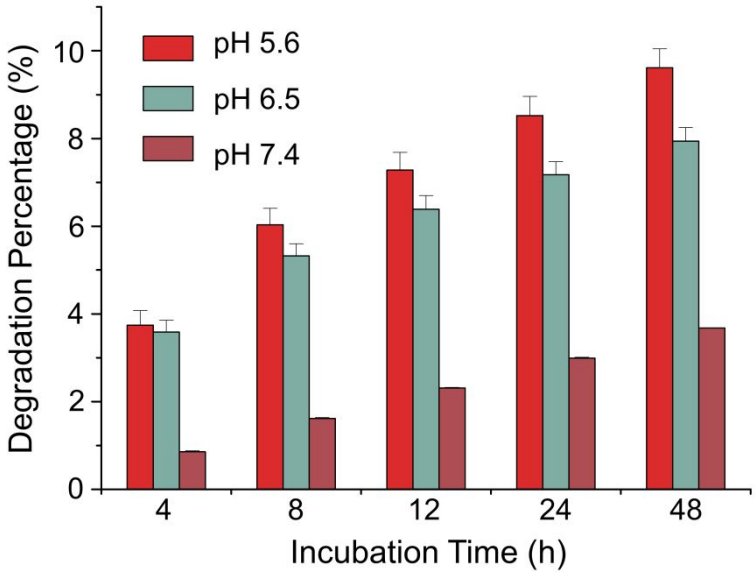

Figure S9. Degradation study of MIL-100 at different pH.

10. UV-Vis Absorption Spectra and LC-MS results of the Curcumin in MCH NPs

The UV-Vis spectra and LC-MS spectra of the curcumin in MCH NPs were evaluated and compared with that of standard curcumin solutions. The results were shown in **Figure S10** and **Figure S11**. The curcumin released from MCH NPs exhibited similar UV-Vis absorption spectrum and LC-MS spectrum with curcumin solutons. These results indicated that the encapsulation of curcumin in the pores of MIL-100 negligibly influence the structure of curcumin, and the coordination interaction between Fe^{3+} and phenolic groups did not impact the release of curcumin from MCH NPs.

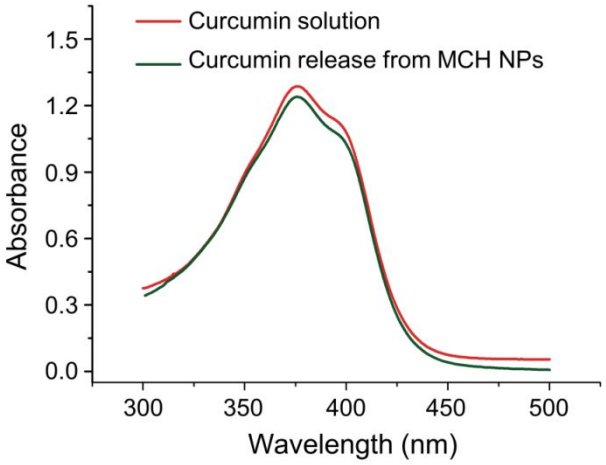

Figure S10. The UV-Vis absorption spectra of curcumin solutions and the curcumin released from MCH NPs.

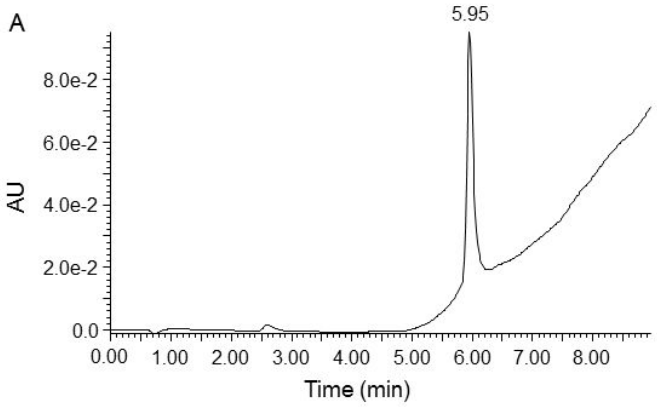

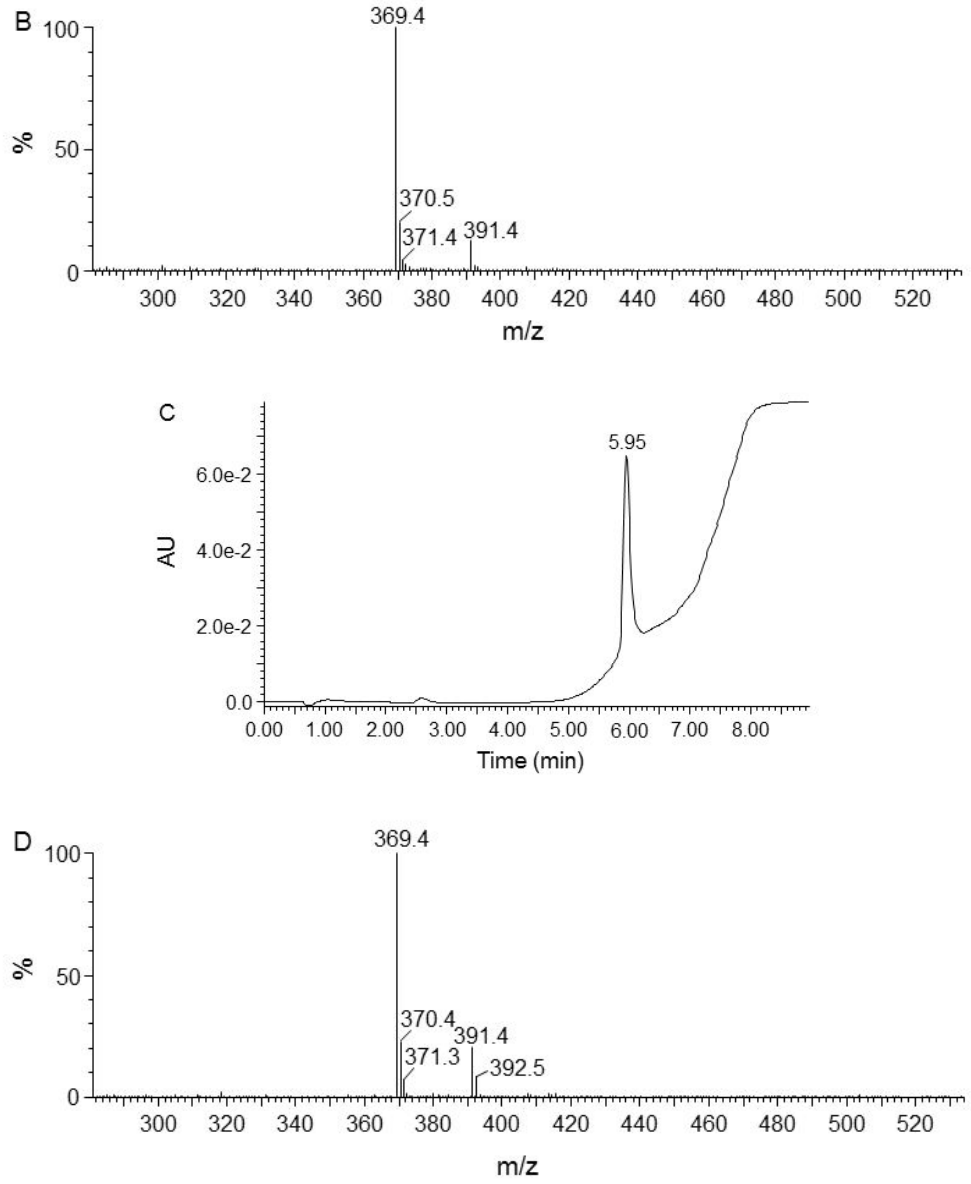

Figure S11. The curcumin solutions and curcumin in MCH NPs were analyzed by LC-MS. The (A) liquid chromatogram and (B) mass spectrum of curcumin solutions. The (C) liquid chromatogram and (D) mass spectrum of the curcumin in MCH NPs.

11. Photothermal Conversion Curves of MCH NPs at Different pH

For MCH NPs, the photothermal conversional ability slightly decreased after incubation at acidic conditions for 24 h (**Figure S12**). After 24 h of incubation at pH 5.6, MCH NPs solution exhibited a temperature increase of 29.7 ^{o}C after 6 min of 808 nm laser irradiation (1 W/cm^2), which was weaker than that incubated at pH 7.4. This could be ascribed to the sustaining release of curcumin from MCH NPs. However, the sustaining curcumin release only induced a slight decrease of photothermal conversion ability on MCH NPs at acidic conditions, which would not strongly impact the therapeutic outcome.

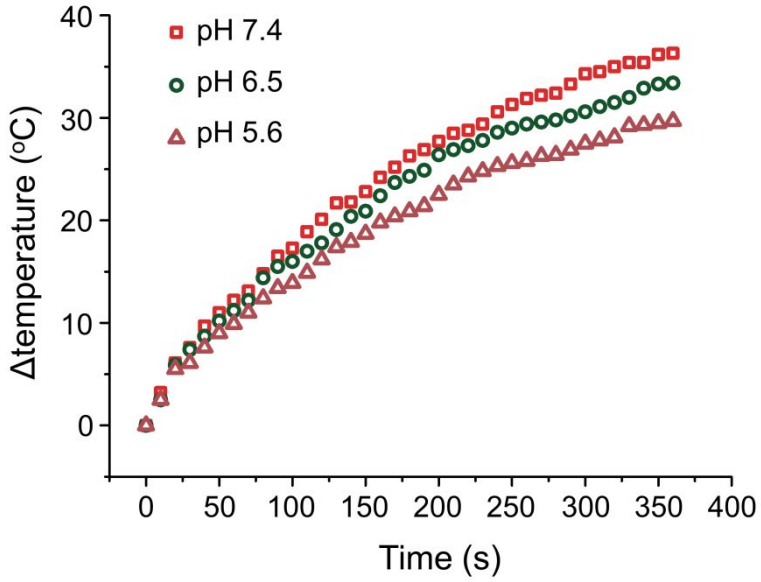

Figure S12. The photothermal curves of MCH NPs after incubation at pH 7.4, 6.5 and 5.6 for 24 h.

12. Cellular Uptake in A549 Cells and MCR-5 Cells

The cellular uptake of MCH NPs in A549 cells and MRC-5 cells was studied by quantificationally analyzing the intracellular curcumin after the cells treated with NPs (**Figure S13**). Compared with curcumin treatment, MC NPs treated A549 cells and MRC-5 cells showed enhanced amount of intracellular curcumin. However, there was a significant distinction between the intracellular curcumin amount of A549 cells and MRC-5 cells after MCH NPs incubation. MCH NPs exhibited further improved cellular uptake toward A549 cells yet feeble cellular uptake toward MRC-5 cells compared with the cells treated with MC NPs. Since tumorous A549 cells were overexpressed with CD44 receptors compared with normal MRC-5 cells, these results suggested the CD44 receptor targeting ability of MCH NPs.

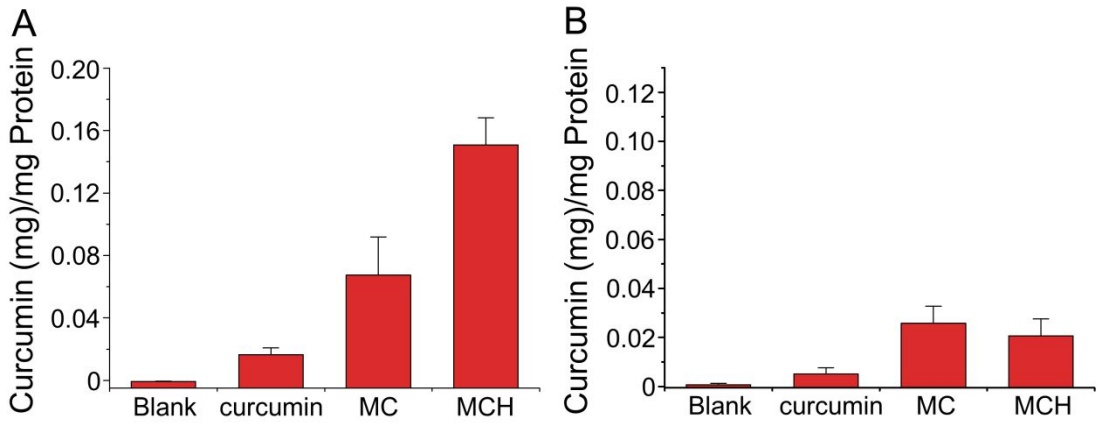

Figure S13. The amount of curcumin uptake by (A) A549 cells and (B) MRC-5 cells after incubation with curcumin, MC NPs and MCH NPs for 4 h.

13. Competitive HA Blocking Experiments

The competitive HA blocking experiments were conducted by quantificationally analyzing the intracellular curcumin of the HA pre-incubated cells after treated with MCH NPs (**Figure S14**). For the tumorous HeLa cells and A549 cells that overexpressed with CD44 receptors, the cellular uptake was weakened as increased amount of HA pre-incubated. However, the HA pre-incubation exhibited negligible influence on the cellular uptake of CHO cells and MRC-5 cells toward MCH NPs. These results could further determine the CD44 receptor targeting ability of MCH NPs.

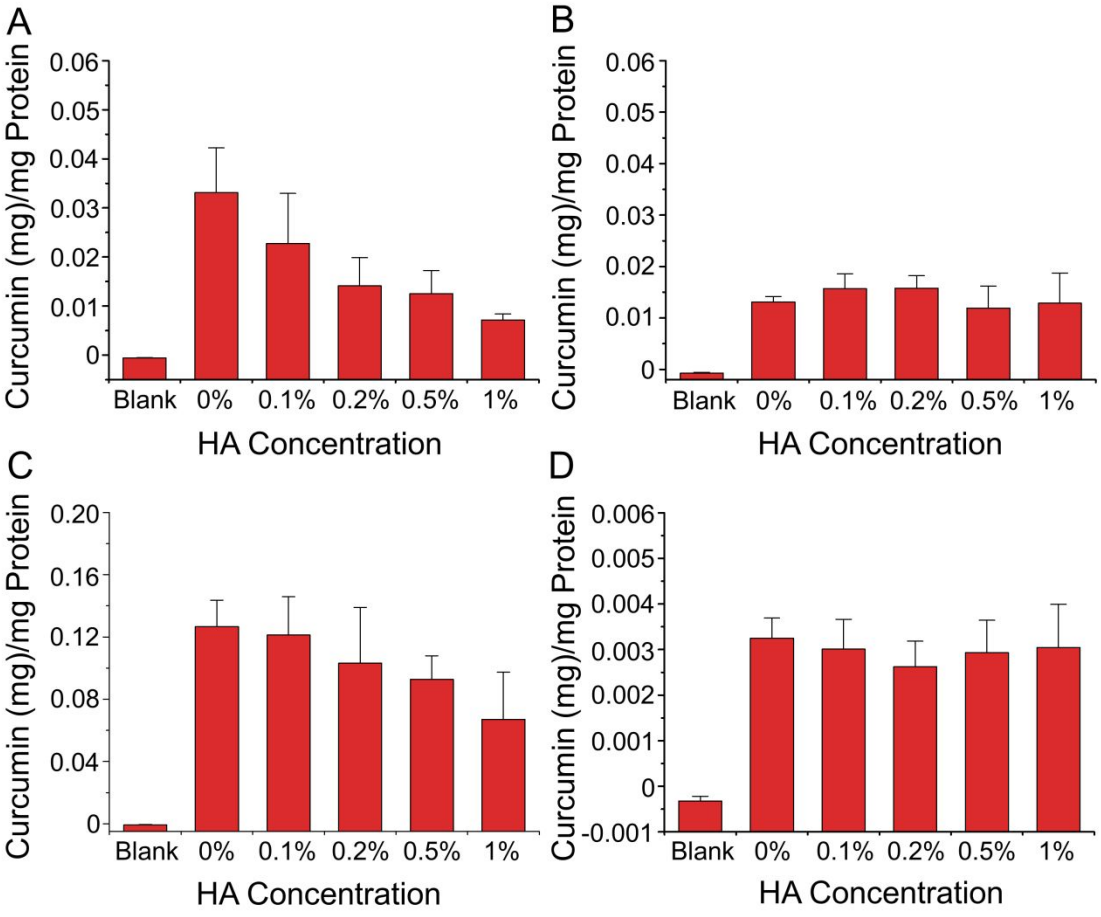

Figure S14. The amount of intracellular curcumin after the pre-incubated (A) HeLa cells, (B) CHO cells, (C) A549 cells and (D) MRC-5 cells treated with MCH NPs.

14. Flow Cytometry in A549 Cells and MRC-5 Cells

Flow cytometry was further employed to evaluate the cellular uptake of MCH NPs (**Figure S15**). After 4 h of incubation, higher cellular uptake was detected in both of A549 cells and MRC-5 cells after treated with MC NPs compared with that treated with curcumin. MCH NPs exhibited further increased cellular uptake in A549 cells compared with MC NPs. However, MCH NPs showed similar cellular internalization in MRC-5 cells to MC NPs. These results were corresponded with those in **Figure S13**, indicating that the improvement of curcumin cellular uptake could be ascribed to the MIL-100 encapsulation and CD44 receptor-mediated endocytosis.

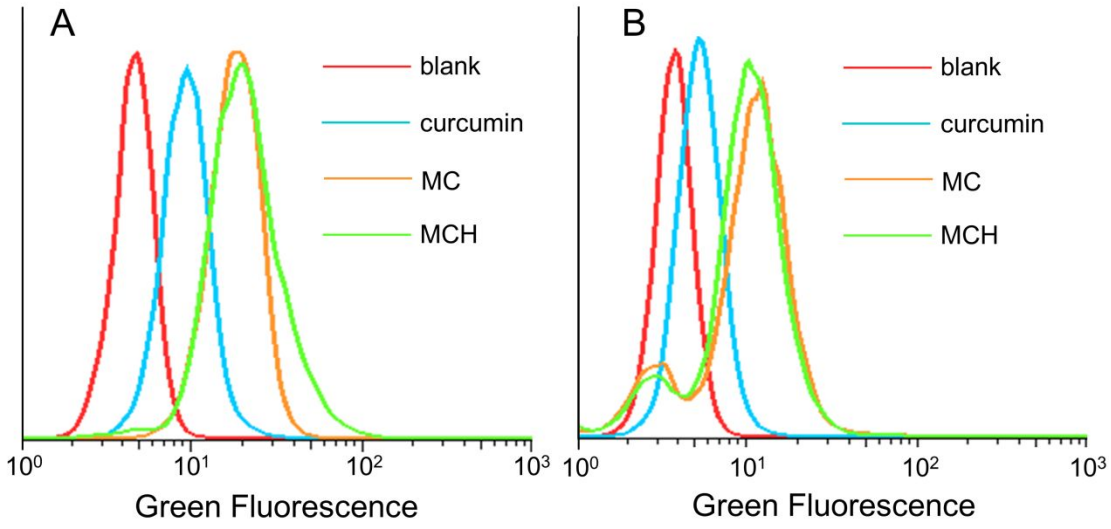

Figure 15. Flow cytometry of (A) A549 cells and (B) MRC-5 cells treated with curcumin, MC NPs and MCH NPs.

15. The Cytotoxicity of Materials in MCH NPs

The cytotoxicity of the constituents in MCH NPs was evaluated in HeLa cells, CHO cells, A549 cells and MRC-5 cells (**Figure S16**, **Figure S17**, **Figure S18** and **Figure S19**). After incubation with different amount of MIL-100, BTC, $FeCl_3 \cdot 6H_2O$ or HA-PDA for 72 h, the cell viability was all higher than 80%, indicating that both the constituents and degradation products of MCH NPs exhibited good biocompatibility.

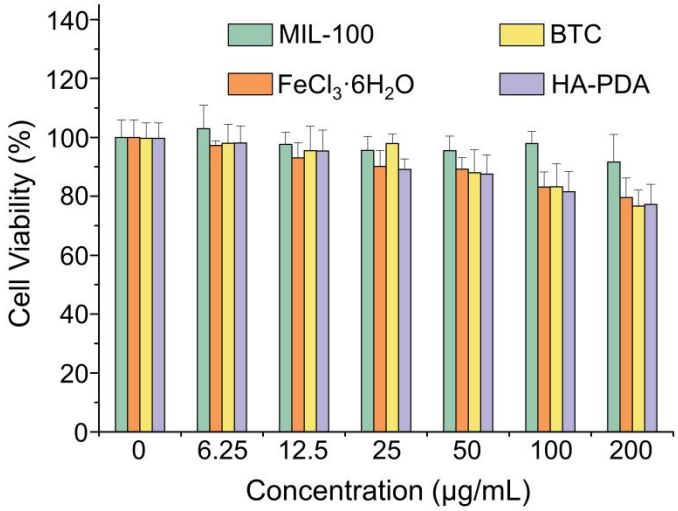

Figure S16. Cell viability of HeLa cells after treated with MIL-100, BTC, $FeCl_3 \cdot 6H_2O$ or HA-PDA for 72 h.

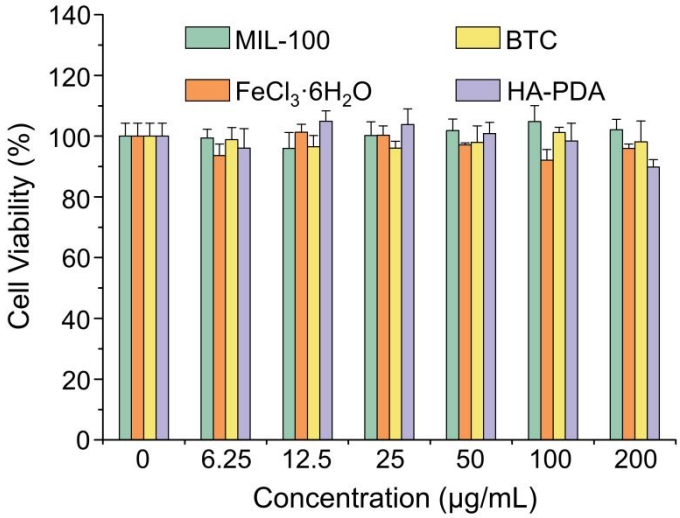

Figure S17. Cell viability of CHO cells after treated with MIL-100, BTC, $FeCl_3 \cdot 6H_2O$ or

HA-PDA for 72 h.

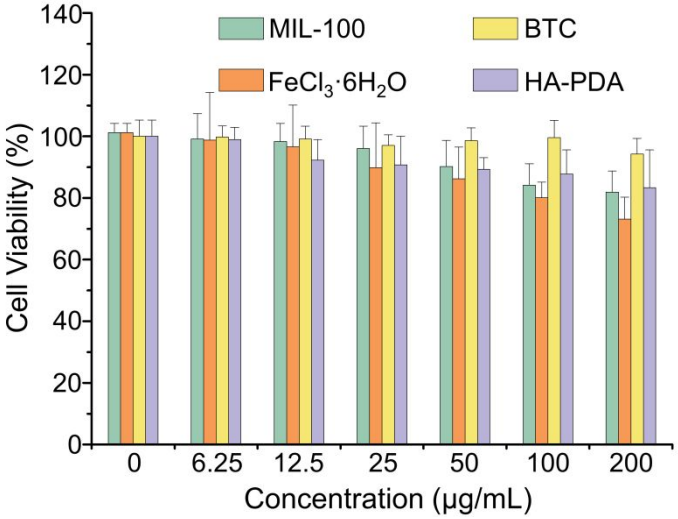

Figure S18. Cell viability of A549 cells after treated with MIL-100, BTC, $FeCl_3 \cdot 6H_2O$ or HA-PDA for 72 h.

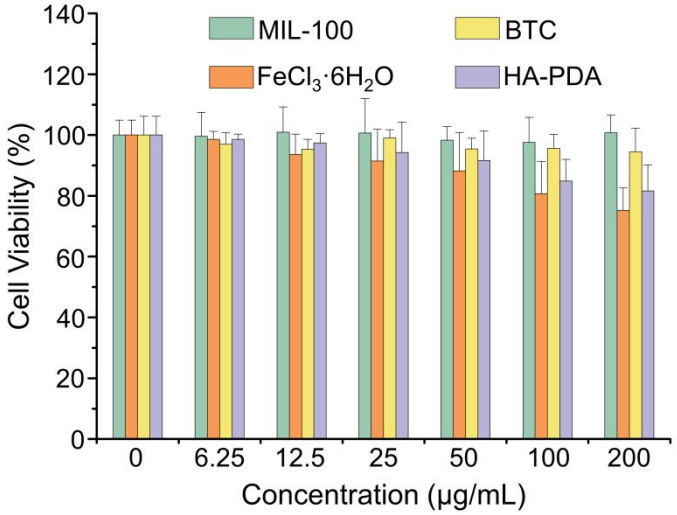

Figure S19. Cell viability of MRC-5 cells after treated with MIL-100, BTC, $FeCl_3 \cdot 6H_2O$ or HA-PDA for 72 h.

16. The Cytotoxicity of MCH NPs in A549 Cells and MRC-5 Cells

The cytotoxicity of MCH NPs was investigated in A549 cells and MRC-5 cells after incubation for 72 h (**Figure S20** and **Figure S21**). These results indicated that MCH NPs exhibited considerable chemotherapy cytotoxicity compared with curcumin.

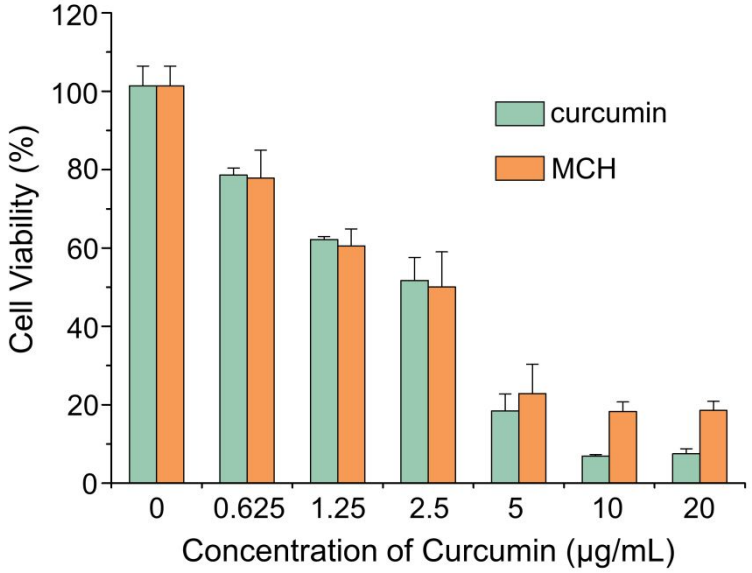

Figure S20. Cell viability of A549 cells after treated with curcumin or MCH NPs for 72 h.

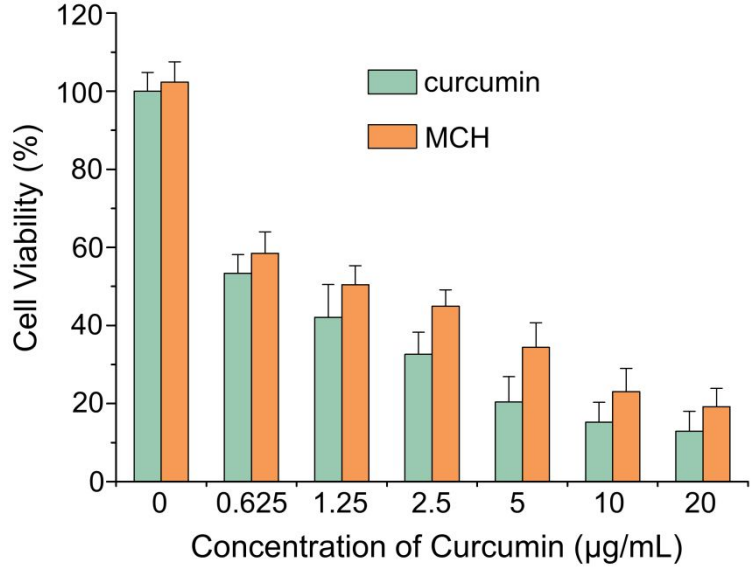

Figure S21. Cell viability of MRC-5 cells after treated with curcumin or MCH NPs for 72 h.

17. Influence of Fe^{3+} toward Cytotoxicity of Curcumin

Since Fe^{3+} could release from MIL-100 under acidic conditions, it may specifically interact with curcumin and then influence the cytotoxicity of curcumin. With this concern, we evaluated the cytotoxicity of curcumin with the presence of different amount of $FeCl_3 \cdot 6H_2O$ in HeLa cells. The results in **Figure S22** indicated that, the presence of Fe^{3+} showed negligible influence toward the cytotoxicity of curcumin. So it could be inferred that, MIL-100, as the vector to load curcumin, would not decrease the chemotherapeutic capability of curcumin.

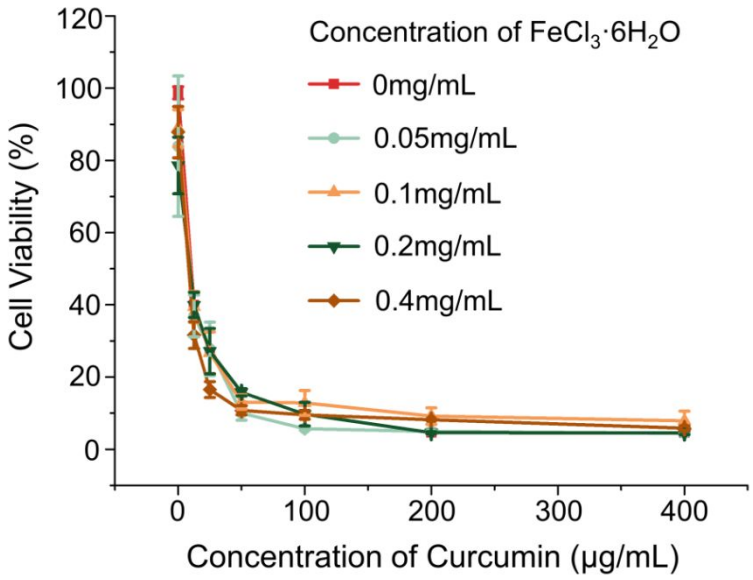

Figure S22. Cell viability of HeLa cells treated with curcumin in the absence of different concentration of $FeCl_3 \cdot 6H_2O$.

18. Chemo/photothermal Combinational Therapy of MCH NPs in A549 cells and MRC-5 cells

The chemo/photothermal combinational therapy capability of MC NPs and MCH NPs was assessed on A549 cells and MRC-5 cells under 808 nm laser irradiation (1.0 W/cm^2). Without 808 nm laser irradiation, the cells exhibited cell viability ranging from 20% to 90% after incubated with MC NPs or MCH NPs for 24 h, which was induced by the sustaining curcumin release from MC NPs and MCH NPs. When irradiated with an 808 nm laser (1 W/cm^2, 5 min), the cells treated with MC NPs or MCH NPs showed much lower survival rates compared with the non-irradiated cells, indicating the considerable chemo/photothermal combinational therapy capability of MC NPs and MCH NPs (**Figure S23** and **Figure S24**).

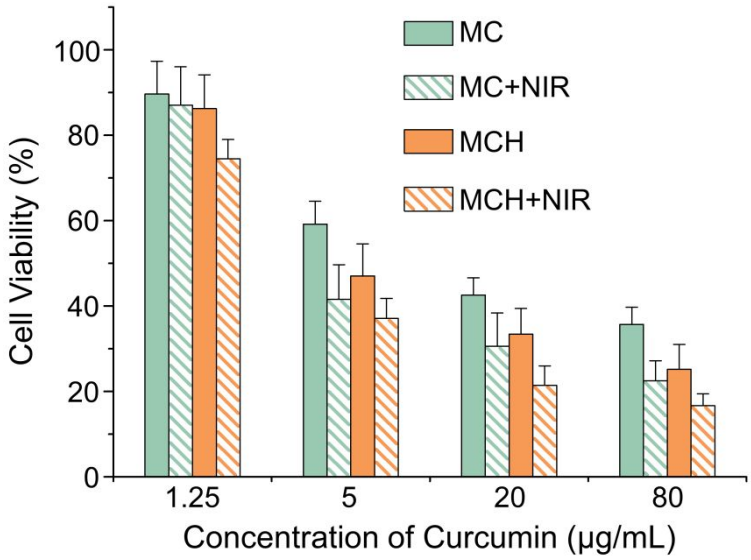

Figure S23. Cell viability of A549 cells after treated with MC or MCH NPs with (or without) 808 nm laser (1 W/cm^2) irradiation.

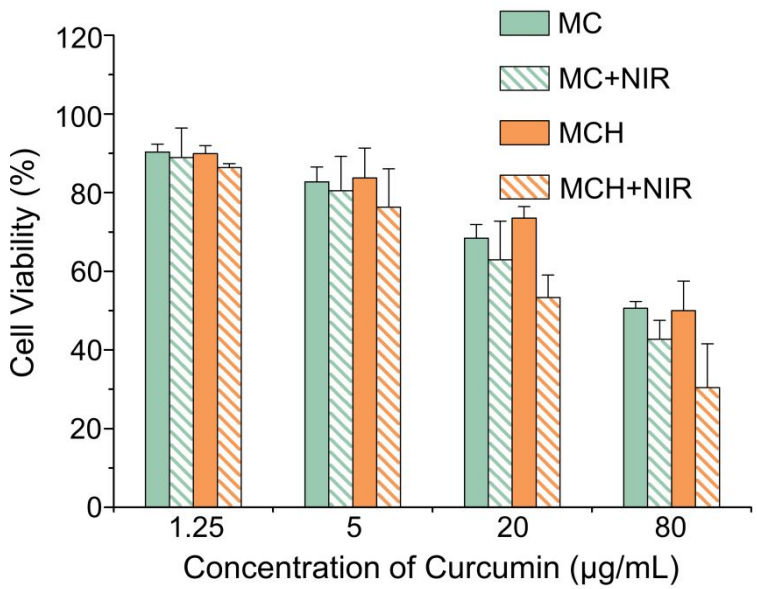

Figure S24. Cell viability of MRC-5 cells after treated with MC or MCH NPs with (or without) 808 nm laser (1 W/cm^2) irradiation.

19. Cytotoxicity of MC NPs and MCH NPs in Normal Cells

The cytotoxicity of MC NPs and MCH NPs was evaluated in CHO cells. The results were shown in **Figure S25**. After 12 h of incubation, both MC NPs and MCH NPs exhibited considerable cytotoxicity. And the cytotoxicity of MCH NPs was lower than that of MC NPs.

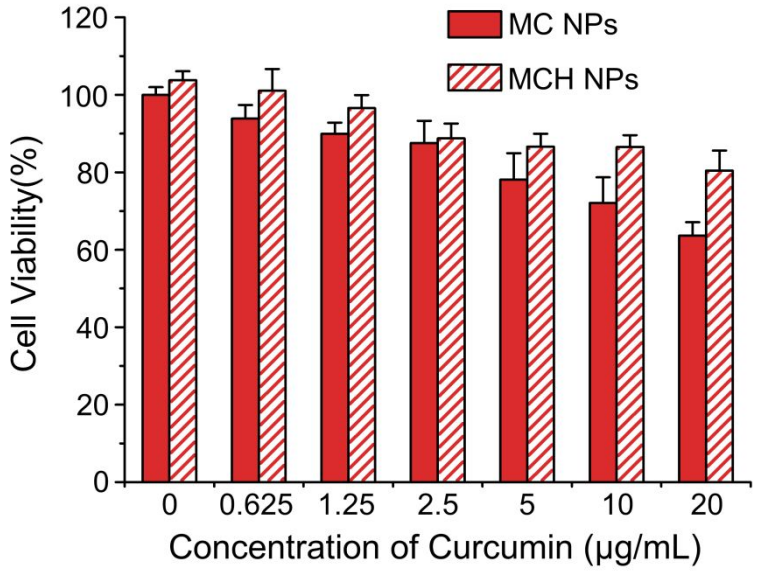

Figure S25. Cell viability of CHO cells after incubated with different concentration of MC NPs or MCH NPs for 12 h.

20. Curcumin Release in FBS and PBS Medium

The release of curcumin from MCH NPs was assessed in FBS and PBS medium at pH 7.4. From the results in **Figure S26**, it could be inferred that MCH NPs have a negligible curcumin release in FBS medium. And in PBS medium (pH 7.4), there was nearly no curcumin released from MCH NPs during 48 h of incubation (**Figure S27**). These results indicated that the curcumin release would be negligible during the circulation of MCH NPs in the blood.

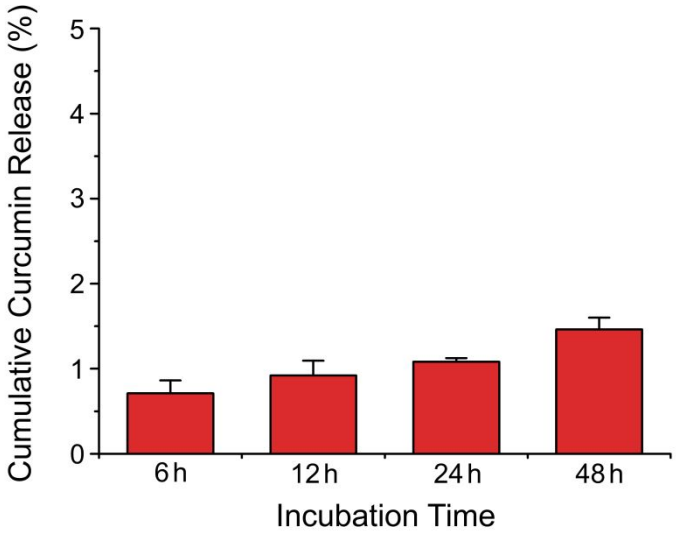

Figure S26. Cumulative curcumin release from MCH NPs in FBS at pH 7.4.

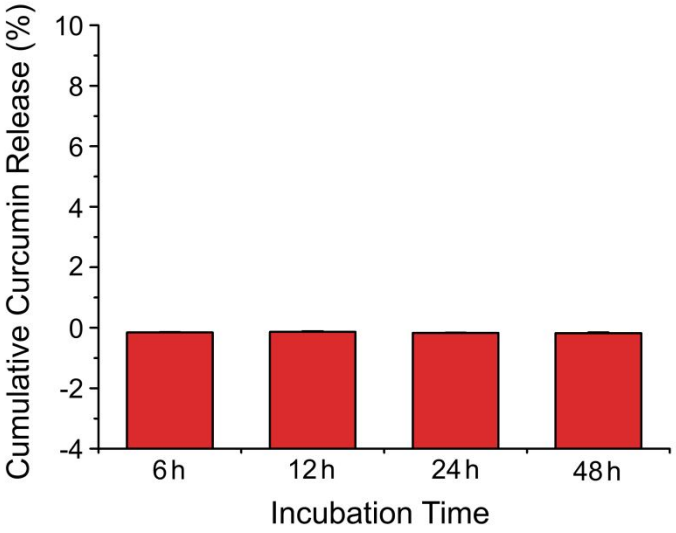

Figure S27. Cumulative curcumin release from MCH NPs in PBS at pH 7.4.

21. Stability In Vivo

By monitering the concentration of Fe^{3+} in the blood after the mice were injected with MC NPs or MCH NPs for different time, the stability of MC NPs and MCH NPs were compared in vivo. From the results shown in **Figure S28**, it could be inferred that MCH NPs exhibited longer circulation time in vivo compared to MC NPs. The pharmacokinetic profile fit a two-compartment model. By calculation, MCH NPs showed a distribution half-life ($t_{1/2\alpha}$) of 2.10 h and a blood-elimination half-life ($t_{1/2\beta}$) of 18.66 h. And for MC NPs, the distribution half-life ($t_{1/2\alpha}$) was 0.92 h and the blood-elimination half-life ($t_{1/2\beta}$) was 4.27 h, which was lower than those of MCH NPs. These results indicated the excellent stability of MCH NPs in vivo.

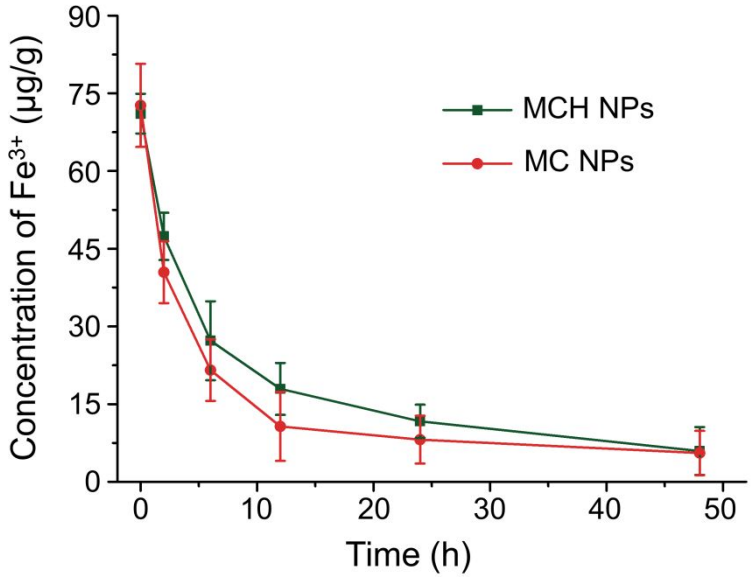

Figure S28. Pharmacokinetics study of MC NPs and MCH NPs after intravenous injection.

22. The Photothermal Effect In Vivo

To evaluate the photothermal effect of NPs in vivo, the tumor temperature was recorded with an infrared thermographic camera at different time intervals under 808 nm laser irradiation at 24 h post-injection (**Figure S29**). The tumor temperature of MCH NPs injected mice rapidly increased to 55.1 °C with 808 nm laser irradiation (1 W/cm^2) for 10 min. Meanwhile, for MH NPs (MIL-100 coated with HA-PDA) injected mice, the tumor temperature only increased to 50.2 °C. Then, with an increased power of 808 nm laser irradiation (1.2 W/cm^2) for 10 min, the tumor temperature of the MH NPs injected mice increased to 55.0 °C, which was approximate to that of MCH NPs group.

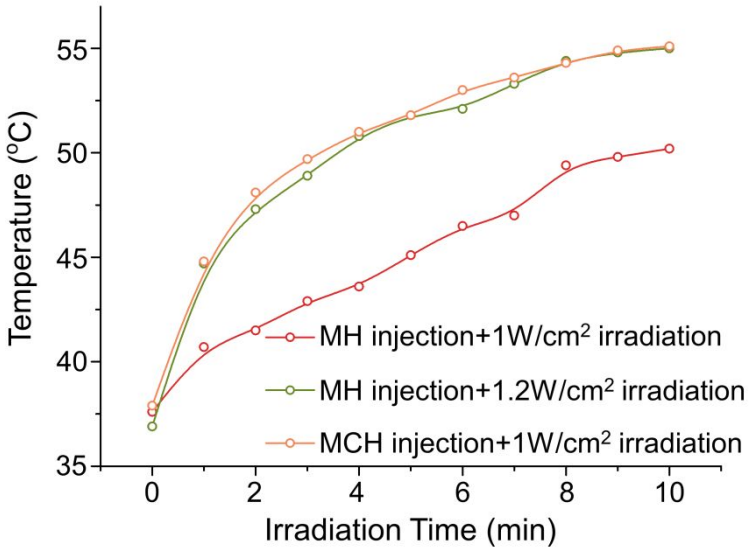

Figure S29. The tumor site temperature change of the mice bearing HeLa tumors post-injected with different kinds of nanoparticles for 24 h and irradiated under different conditions.

23. H&E Staining Images

The organs and tumors excised from the mice were further investigated by H&E staining (**Figure S29**). For the mice injected with PBS and curcumin, nearly no apparent tumor cell destruction could be observed. And weak tumor necrosis was observed in the mice injected with MCH NPs and the mice injected with MH NPs and then irradiated with 808 nm laser (1.2 W/cm^2). By contrast, the mice injected with MCH NPs and irradiated with 808 nm laser (1.0 W/cm^2) showed apparent tumor necrosis. Furthermore, the H&E images of major organs (heart, liver, spleen, lung, and kidney) indicated that no evident damage was induced by the NPs or laser irradiation.

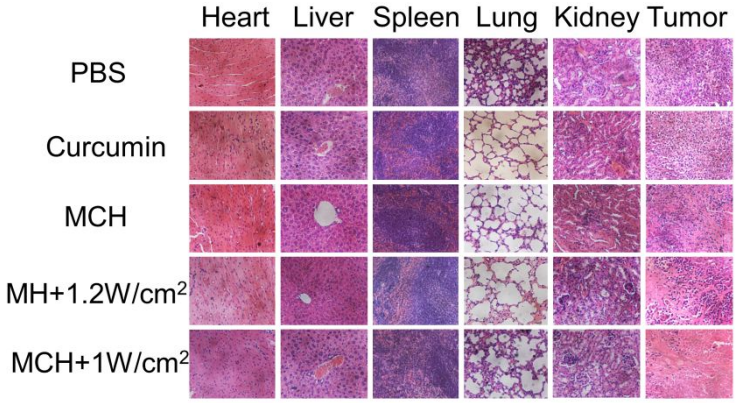

Figure S29. H&E staining images of the mice with different treatment.

Table S1. The particle size of the products obtained by microwave-assisted interaction between $FeCl_3 \cdot 6H_2O$ and trimesic acid with different molar ratios.

Molar ratio of $FeCl_3 \cdot 6H_2O$/BTC Feeding ratio	Particle size of product (nm)
9:4	1770.1 ± 72.5
9:3	302.0 ± 28.7
9:2	194.1 ± 4.8
9:1	281.3 ± 4.2

Table S2. Drug loading contents and drug loading efficiency of the obtained MC NPs by incubating MIL-100 and curcumin with different weight ratio.

MIL-100/curcumin (w/w)	Drug loading content (%)	Drug loading efficiency (%)
1/2	42.1	36.3
1/1	33.3	49.9
1/0.5	33.0	94.3
1/0.25	18.5	91.1
1/0.125	9.4	82.6

Table S3. The Fe elemental analysis results of MIL-100, MC NPs and MCH NPs.

Sample	Content of Fe element (%)
MIL-100	18.3
MC	12.7
MCH	3.7